Solid State Communications 152 (2012) 204–209

Contents lists available at SciVerse ScienceDirect

Solid State Communications

journal homepage: www.elsevier.com/locate/ssc

Measurement of the absolute Raman cross section of the optical phonons in type Ia natural diamond

R.L. Aggarwal [a,*], L.W. Farrar [a], S.K. Saikin [b], X. Andrade [b], A. Aspuru-Guzik [b], D.L. Polla [c]

[a] MIT Lincoln Laboratory, Lexington, MA 02420-9108, USA

[b] Department of Chemistry and Chemical Biology, Harvard University, Cambridge, MA 02138, USA

[c] College of Science and Engineering, University of Minnesota, Minneapolis, MN 55454, USA

ARTICLE INFO

Article history:
Received 2 September 2011
Received in revised form
14 October 2011
Accepted 4 November 2011
by B.-F. Zhu
Available online 19 November 2011

Keywords:
A. Semiconductors
B. Phonons
C. Inelastic light scattering

ABSTRACT

The absolute Raman cross section σ_{RS} of the first-order 1332-cm^{-1} optical phonons in type Ia natural diamond was measured using 785- and 1064-nm pump lasers for the excitation of Raman scattering. A small temperature-controlled blackbody was used for the signal calibration of the 785- and 1064-nm Raman systems. Measurements were made with a 0.9-mm thick (111) natural diamond sample. Values of $2.7 \pm 0.6 \times 10^{-29}$ and $0.95 \pm 0.2 \times 10^{-29}$ cm^2 per carbon atom were determined for σ_{RS} for 785- and 1064-nm excitation, respectively. The corresponding values of the Raman scattering efficiency S are $3.8 \pm 0.8 \times 10^{-7}$ and $1.3 \pm 0.3 \times 10^{-7}$ cm^{-1} sr^{-1}. The values of the Raman polarizability $|d|$ for 785-, and 1064-nm excitation are $6.8 \pm 0.7 \times 10^{-16}$ and $8.1 \pm 0.8 \times 10^{-16}$ cm^2, respectively. Our measured values of $|d|$ are larger than the previously measured values of $4.4 \pm 0.3 \times 10^{-16}$ and $4.6 \pm 0.7 \times 10^{-16}$ cm^2 using 514.5- and 694-nm excitation, respectively. $|d|$ vs. excitation photon energy was computed for the range from 1.0 eV (1240 nm) to 4.0 eV (310 nm) using time-dependent density functional theory. The computed values of 5.8×10^{-16} and 5.3×10^{-16} cm^2 for 514.4- and 694-nm excitation, respectively, are larger than the corresponding measured values of $|d|$. The computed values of 5.2×10^{-16}, and 5.0×10^{-16} cm^2 for 785- and 1064-nm excitation are smaller than the corresponding values of $|d|$ measured in this work. The computed value of $|d|$ in the static limit is 4.7×10^{-16} cm^2. Modification of $|d|$ due to IaA and IaB defects, computed for a 64-atom supercell, is less than 5%.

1. Introduction

In this paper, we report on the *first* measurement of the absolute Raman cross section of the 1332-cm^{-1} mode in type 1a diamonds using 785- and 1064-nm pump lasers for the excitation of Raman scattering and a temperature-calibrated blackbody for the signal calibration of the 785- and 1064-nm Raman systems [1]. The previous absolute Raman cross section measurements were made on Type IIa diamonds. We have also computed the excitation-energy-dependent Raman cross section of the 1332-cm^{-1} mode for the range of excitation energies 1–4 eV as well as in the long-wavelength limit using a *full first-principles approach*, which is based on time-dependent density functional theory (TTDFT) in the local density approximation (LDA) [2]. This is a *state-of-the-art* method used presently to compute properties of materials. Vibrational properties are usually well described by the density functional theory and so is the case for diamond [3]. The results of our measurements and computations are comparable (within a factor of 2) with those of the previous, more accurate measurements by McQuillan et al. in 1970 [4], and Grimsditch and Ramdas in 1975 [5] using Brillouin scattering as the reference. We note that the absolute Raman cross section of any substance (solid, liquid, or gas) can be measured using the blackbody for the signal calibration of the Raman system while Brillouin scattering can be used as a reference only for substances that are crystals.

Diamond, which is known as a girl's best friend, is the hardest natural material known. The relative hardness of diamond is 10 Mohs [6]. The Knoop hardness of diamond is 8000; the Knoop microhardness is 79 GPa [7]. The Young's modulus of diamond along the [111] direction is 1223 GPa [8]. In addition, diamond has interesting optical and thermal properties. Diamond is a large-gap semiconductor with indirect gap of 5.48 eV (226 nm) and direct gap of 7.12 eV (174 nm) [9], and refractive index of 2.41–2.46 for visible light [10]. Furthermore, diamond has large thermal conductivity of 900 W/m K at 300 K and 3000 W/m K at 100 K [11].

The diamond crystal is composed of carbon atoms in a face-centered cubic crystal structure with a basis of two atoms at 000 and 1/4, 1/4, 1/4 associated with each lattice point [12]. There are eight atoms in the cubic unit cell and there are two atoms in the primitive unit cell, which contains lattice points at the corners

* Corresponding author. Tel.: +1 781 981 0626; fax: +1 781 981 0602.
E-mail address: aggarwal@ll.mit.edu (R.L. Aggarwal).

0038-1098/$ – see front matter © 2011 Elsevier Ltd. All rights reserved.
doi:10.1016/j.ssc.2011.11.005

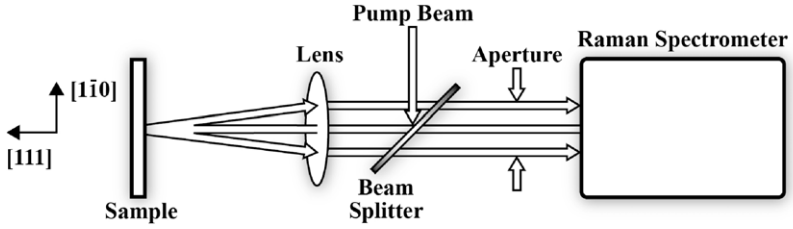

Fig. 1. Schematic of the optical setup for the measurement of Raman cross section; the sample is located in the focal plane of a 20-mm effective focal length (EFL) lens.

only. Each atom has four nearest neighbors bonded in a tetrahedral arrangement with a bond length of 0.15445 nm. The density of diamond is 3.515 g/cm^3, which results in an atomic concentration of 1.762 $\times$ 10^{23} cm^{-3}. The weight of a diamond is expressed in carats. One carat is equal to 200 mg and has a volume of 56.9 mm^3.

There are four types of natural diamonds: (1) type Ia which contains pairs and other aggregates of substitutional nitrogen atoms; (2) type Ib which contains single/isolated substitutional nitrogen atoms; (3) type IIa which is relatively free of nitrogen and other impurities; (4) type IIb which contains substitutional boron atoms.

There are six phonon modes in diamond with two atoms in the primitive unit cell. Three of the phonon modes are triply-degenerate optical (LO + TO) modes, while two of the phonon modes are doubly-degenerate transverse acoustic (TA) modes, and finally, the remaining phonon mode is the longitudinal acoustic (LA) mode. The frequency of the triply-degenerate optical phonon modes is 1332 cm^{-1} [13]. The absolute Raman cross section of the 1332-cm^{-1} mode in diamond was first measured by Anastassakis and Burstein in 1970 [14] using the electric-field induced infrared absorption at 1332-cm^{-1}. The Raman cross section of the 1332-cm^{-1} mode was determined by McQuillan et al. in 1970 [4] using that of benzene as the reference material. The absolute Raman cross section of the 1332-cm^{-1} mode of diamond was measured by Grimsditch and Ramdas in 1975 [5] by comparing the intensity of the Raman scattering with that of the Brillouin scattering. The value of the Raman cross section obtained in Ref. [5] is in good agreement with that obtained in Ref. [4].

2. Experimental details

The diamond sample used in our experiments was a 0.9-mm thick plane parallel plate with faces that are 10° off the [111] crystallographic orientation as determined by the X-ray diffraction measurements.

A schematic of the optical setup is shown in Fig. 1, which includes a Raman spectrometer, a 45° beamsplitter for directing the pump beam onto the sample through the focusing lens that collects as well as collimates the backscattered Raman radiation into the Raman spectrometer. The diameter of the focused pump beam was ~40 μm.

The focusing lens is a 12-mm diameter, 20-mm effective focal length (EFL) near infrared (NIR) achromat Edmund Optics [15] part number 45–792. The 785- and 1064-nm beamsplitters are dichroic and were procured from Chroma Technology [16]. The fraction of the scattered light collected is limited by a 7-mm diameter aperture, which is placed between the beamsplitter and the Raman spectrometer. The 785-nm pump laser is a 1400-mW CW single-mode, linearly polarized Sacher Lasertechnik [17] diode laser model SYS-420-0785-1400. The 1064-nm pump laser is a 10-W CW IPG Photonics [18] linearly polarized fiber laser model YLR-10-1064-LP.

The 785- and 1064-nm Raman spectrometers are DeltaNu [19] model Advantage 785 and 1064, respectively. The Advantage 785 is equipped with a silicon CCD camera MOSIR 350 [20]. The Advantage 1064 is equipped with InGaAs camera MOSIR 950 [20]. The grating in the Advantage 785 has 1800 grooves/mm. The grating in the Advantage 1064 has 830 grooves/mm. Each of the two Raman spectrometers includes two long-wave pass (LWP) filters and a 2× beam expander, which consists of two lenses of 20- and 40-mm EFL. A small pinhole is placed at the common focus of the beam expander to reduce unwanted radiation entering the camera in the Raman spectrometer. The diameter of the pinholes in the 785- and 1064-nm Raman spectrometers is 100 μm.

The Raman spectrometers were calibrated using a 50–1000 °C, small-cavity, blackbody Electro Optical Industries [21] model CS 1000–008 with 85-mil (2.16-mm) aperture. The 85-mil aperture of the blackbody was covered with a 50-μm pinhole, which is comparable in size to that of the focused pump beam. The temperature of the blackbody was set at 675 and 500 °C for the calibration of the 785- and 1064-nm Raman spectrometers, respectively.

3. Theoretical calculations

The polarization unit vector $\mathbf{E_R}$ of the scattered light is related to that of the pump light $\mathbf{E_P}$ as

$$E_R = \frac{1}{d}\chi E_P, \tag{1}$$

where d is the Raman polarizability. χ is the 3 × 3 Raman polarizability tensor. The Raman polarizability tensors for diamond referred to the cubic crystal axes x, y, and z, represented by [100], [010], and [001] respectively, are given by Loudon [22]. For the analysis of the experimental data in this work, it is more convenient to transform χ_1, χ_2, and χ_3 in terms of the x', y', and z' coordinate system, where x', y', and z' are parallel to [1$\bar{1}$0], [11$\bar{2}$], and [111] directions, respectively. Using the transformation rules [23], the transformed Raman polarizability tensors are given by

$$\chi_1' = \begin{bmatrix} 0 & \frac{d}{\sqrt{3}} & -\frac{d}{\sqrt{6}} \\ \frac{d}{\sqrt{3}} & -\frac{2d}{3} & -\frac{d}{3\sqrt{2}} \\ -\frac{d}{\sqrt{6}} & -\frac{d}{3\sqrt{2}} & \frac{2d}{3} \end{bmatrix}, \tag{2}$$

$$\chi_2' = \begin{bmatrix} 0 & -\frac{d}{\sqrt{3}} & \frac{d}{\sqrt{6}} \\ -\frac{d}{\sqrt{3}} & -\frac{2d}{3} & -\frac{d}{3\sqrt{2}} \\ \frac{d}{\sqrt{6}} & -\frac{d}{3\sqrt{2}} & \frac{2d}{3} \end{bmatrix}, \tag{3}$$

$$\chi_3' = \begin{bmatrix} -d & 0 & 0 \\ 0 & \frac{d}{3} & \frac{\sqrt{2}d}{3} \\ 0 & \frac{\sqrt{2}d}{3} & \frac{2d}{3} \end{bmatrix}. \tag{4}$$

In this experiment, the pump and scattered beams propagate along the z'-axis. Therefore, the z'-components of $\mathbf{E_P}$ and $\mathbf{E_R}$ must be zero. Using Eqs. (1)–(4), Raman signal is given by

$$I_R \propto \frac{5d^2}{3}, \tag{5}$$

irrespective of the pump beam polarization. The Raman collection efficiency is given by

$$\eta_c = \frac{D_A^2}{16n^2(\mathrm{EFL})^2}, \tag{6}$$

where D_A is the diameter of the aperture placed between the beamsplitter and the Raman spectrometer and n is the refractive index of the sample at the wavelength of the scattered light. The value of D_A is 7 mm. The Raman cross section is given by

$$\sigma_{RS} = \frac{Fh\nu_P}{\eta_c P_P NL}, \tag{7}$$

where F is the integrated area under the Raman mode, $h\nu_P$ is the pump photon energy, P_P is the pump power incident upon the sample, N is the atomic concentration of diamond, and L is the effective thickness that contributes to scattering [1]. Several authors use Raman scattering efficiency S per unit length per unit solid angle, which is related to σ_{RS} as follows:

$$S = \frac{\sigma_{RS}N}{4\pi}. \tag{8}$$

The magnitude of the Raman polarizability $|d|$ is related to the average value of σ_{RS} for $\mathbf{E_P}$ parallel and perpendicular to the x'-axis as

$$|d| = \left(\frac{3}{5}\right)^{\frac{1}{2}} \left(\frac{\rho c^4 \nu_R \sigma_{RS}}{8\pi^3 h \nu_S^4 N(n_0+1)}\right)^{\frac{1}{2}}, \tag{9}$$

where the factor $(3/5)^{1/2}$ accounts for the fact that Raman intensity is proportional to $(5/3)d^2$ for backscattering along the [111] direction, ρ is the mass density, ν_R is Raman frequency (Hz) of the optical phonon mode, h is the Planck constant, ν_S is the frequency (Hz) of the Stokes component of the Raman scattered light, and n_0 is the optical phonon occupation number.

The Raman polarizability in the static limit has been computed using Quantum Espresso code [24,25] and the excitation-energy-dependent calculations have been made with the Octopus code [26]. Both the static and dynamic calculations were performed using the local density approximation (LDA) to the exchange and correlation energy and norm-conserving pseudopotentials [27]. The value of the lattice constant a used in the calculations was 3.565 Å and the value of atomic mass of carbon was 12.011 amu. The static calculations were done in a plane-wave basis with the energy cutoff equal to 90 Ry. The irreducible part of the Brillouin zone was sampled with 2480 wave vectors spaced on a uniform grid.

The results for finite excitation energies were obtained by calculating the dynamical susceptibility for distorted geometries as described in Refs. [28,29]. We used a displacement δ equal to $0.001a$ along the trigonal axis. The dynamical susceptibilities were calculated in the time-dependent density functional theory (TDDFT) framework using a real-time approach and a vector potential representation for the electric field [2]. The simulation was done with 8 atoms per unit cell, a shifted uniform grid of 512 K-points and a grid spacing of 0.11 Å (equivalent to 222 Ry). The external vector potential intensity was 0.1 a.u. The total propagation time was 12 fs with a time-step of 0.006 fs.

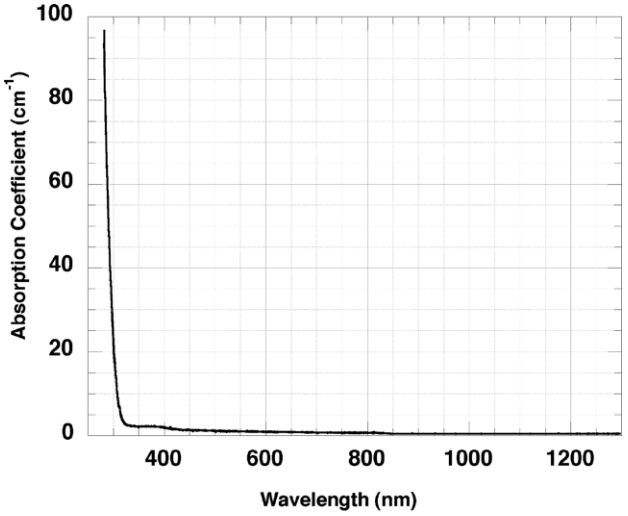

Fig. 2. UV–V–NIR absorption spectrum of the 0.9-mm thick (111) diamond sample obtained using Perkin–Elmer spectrometer 950.

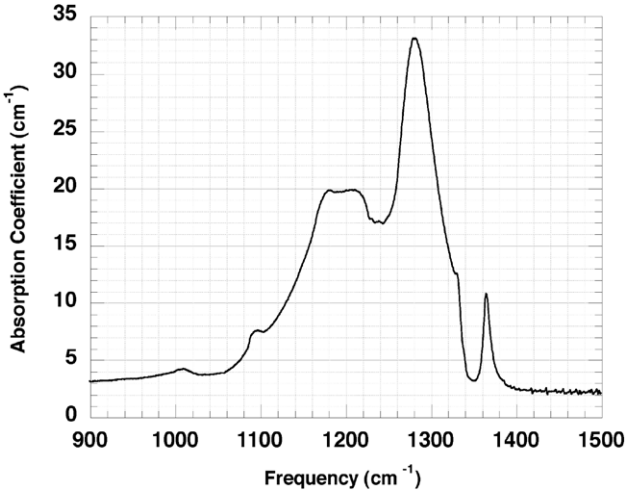

Fig. 3. IR absorption spectrum of the 0.9-mm thick (111) diamond sample obtained with a spectral resolution of 2 cm^{-1} using Fourier transform infrared (FTIR) spectrometer Nicolet 4700.

4. Results and discussion

4.1. UV–V–NIR and IR absorption spectra

Fig. 2shows the UV–V–NIR absorption spectrum of our sample for the 285–1300 nm region obtained using Perkin–Elmer spectrometer 950. The absorption is negligible in the ∼325–1300-nm spectral region. The fundamental absorption edge is observed to shift from 226 nm (5.48 eV) in type IaB, Ib, IIa, and IIb diamonds to longer wavelength at ∼280 nm (∼4.4 eV) in Fig. 2. This implies that our sample is type IaA diamond [30,31].

Fig. 3 shows the IR absorption spectrum for the 900–1500 cm^{-1} region with a spectral resolution of 2 cm^{-1} obtained using Fourier transform infrared (FTIR) spectrometer Nicolet 4700 equipped with a ZuSe beam splitter.

Absorption peaks are observed at 1010, 1090, ∼1200, 1282, 1332, and 1365 cm^{-1}. The absorption peaks at 1090, ∼1200, and 1282 cm^{-1} correspond to nitrogen in the A form [31,32]. The absorption peak at 1365, called B', is due to platelet defects on (001) planes [32,33]. The absorption peak at 1332 cm^{-1} is due to the forbidden optical phonon; the selection rule is somewhat relaxed by the nitrogen and other defects in the sample. Using the observed

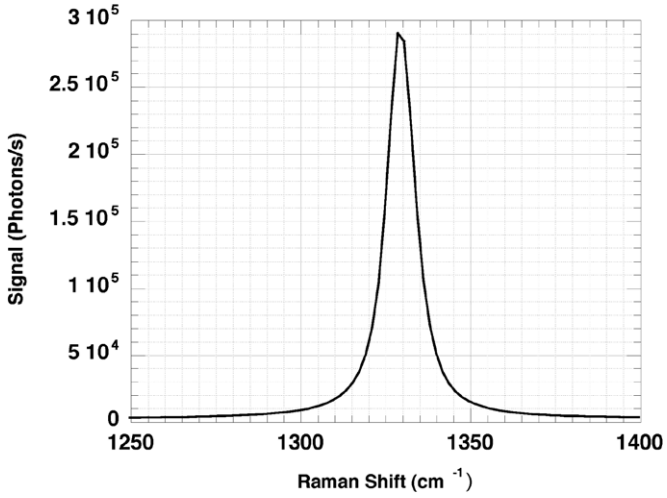

Fig. 4. Raman spectrum of a 0.9-mm thick (111) diamond obtained with 1.0 mW of 785-nm excitation and 1.0-s integration time.

value of ∼31 cm^{-1} (above the background level) for the absorption coefficient of the 1282 cm^{-1} peak, we obtain a value of ∼540 ppm for the atomic concentration of nitrogen in the A form [32].

4.2. 785-nm excitation

Fig. 4 shows the first-order Raman spectrum of the 1332-cm^{-1} optical phonons in diamond obtained with 1.0 mW of 785-nm pump power incident on the sample and 1.0-s integration time.

Using a value of 2.396 for the refractive index [9], we deduce a value of 0.85 mm for the effective sample thickness L. Using a value of 7 mm for D_A, 2.40 for n, and 20 mm for EFL, Eq. (6) yields a value of 1.33×10^{-3} for η_c. The value of F for the 1332-cm^{-1} mode in the spectrum of Fig. 4 is determined to be 2.13×10^6 using 1251–1399 cm^{-1} integration. Using this value of F, 2.527×10^{-19} J for $h\nu_P$, 1.33×10^{-3} for η_c, 1.0 mW for P_P, and 0.85 mm for L, Eq. (7) yields a value of $2.7 \pm 0.6 \times 10^{-29}$ cm^2 per atom for σ_{RS}. Using this value of σ_{RS} and Eqs. (8) and (9), we obtain values of $3.8 \pm 0.8 \times 10^{-7}$ cm^{-1} sr^{-1} and $6.8 \pm 0.7 \times 10^{-16}$ cm^2 for S and $|d|$, respectively. Our measured value of $6.8 \pm 0.7 \times 10^{-16}$ cm^2 for $|d|$ is larger than the calculated value of 5.2×10^{-16} cm^2 for 1.58-eV excitation.

4.3. 1064-nm excitation

Fig. 5 shows the first-order Raman spectrum of the 1332-cm^{-1} mode obtained with 30 mW of 785-nm pump power incident on the sample and 1.0-s integration time.

The value of F for the optical phonon modes in Fig. 5 is determined to be 3.06×10^7 using an integration between 1280–1389 cm^{-1}. Using this value of F, 1.865×10^{-19} J for $h\nu_P$, 1.34×10^{-3} for η_c, 30 mW for P_P, and 0.85 mm for L, Eq. (7) yields a value of $0.95 \pm 0.2 \times 10^{-29}$ cm^2 per atom for σ_{RS}. Subsequently, employing the value of σ_{RS} and Eqs. (8) and (9), we obtain values of $1.3 \pm 0.3 \times 10^{-7}$ cm^{-1} sr^{-1} and $8.1 \pm 0.8 \times 10^{-16}$ cm^2 for S and $|d|$, respectively. Our measured value of $8.1 \pm 0.8 \times 10^{-16}$ cm^2 for $|d|$ is larger than the corresponding computed value of 5.0×10^{-16} cm^2. The value of $|d|$ measured with 1064-nm excitation is higher than that measured with 785-nm excitation; this is inconsistent with the expected dispersion of $|d|$. However, the measured values of $|d|$ may be considered to be nearly the same considering the error bars of the measured data.

Our measured values of σ_{RS}, S, and $|d|$ as well as those from Refs. [3,4] are given in Table 1. The value of S given in Ref. [3] was used to obtain the value of σ_{RS} given in Table 1. The value of $|d|$ given in Ref. [4] was used to obtain the values of σ_{RS} and S given in Table 1.

4.4. Computation

The computed value of $|d|$ in the static limit is 4.7×10^{-16} cm^2, which is 4.5× smaller than the corresponding value of 2.1×10^{-15} cm^2 for the 519-cm^{-1} mode of silicon. The value of 3.0×10^{-15} cm^2 for $|d|$ of silicon given in Ref. [34] is in error by a factor of $\sqrt{2}$.

In general, TDDFT calculations in the LDA approximation can have problems to reproduce some properties of extended systems, in particular the band gap and excitonic effects [33]. For frequencies sufficiently below the gap these errors are reflected in the larger values of system polarizability as compared to experimental data [35]. For this particular case, we can get an idea of the overestimation by comparing the dielectric constant. The computed value of the dielectric constant is 5.8 while the experimental value of the dielectric constant of type IIa diamond is 5.66 ± 0.04 [36], which implies an overestimation of less than 3.0%. Additionally, the predicted LDA dielectric function for diamond has been reported to be close to the experimental one, especially for low frequencies [29]. The vibrational properties of diamond are

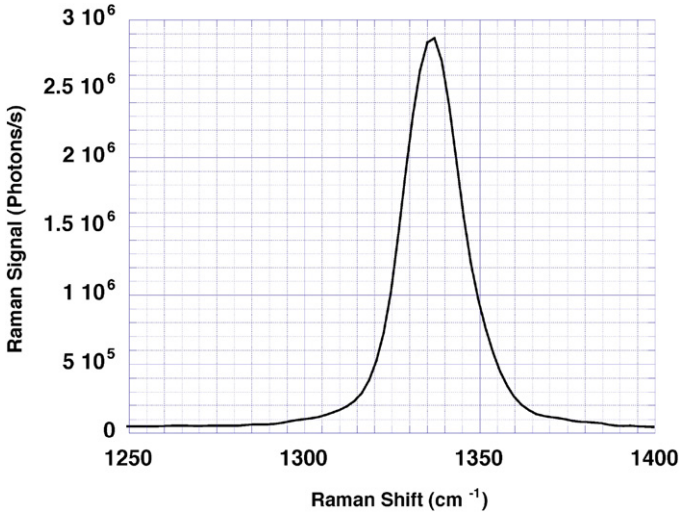

Fig. 5. Raman spectrum of a 0.9-mm thick (111) diamond obtained with 30 mW of 1064-nm excitation and 1.0-s integration time.

Table 1
Summary of the measured values of σ_{RS}, S and $|d|$, and the computed value of $|d|$.

$h\nu_P$ (eV)	σ_{RS} (10^{-29} cm^2) per atom	S (10^{-7} cm^{-1} sr^{-1})	$\|d\|$ (10^{-16} cm^2) Measured	$\|d\|$ (10^{-16} cm^2) Computed
1.165 (1064 nm) (This work)	0.95 ±0.2	1.3 ± 0.3	8.1 ± 0.8	5.0
1.580 (785 nm) (This work)	2.7 ± 0.6	3.8 ± 0.8	6.8 ± 0.7	5.2
1.787 (694 nm) (Ref. [3])	1.9 ± 0.6	2.7 ± 0.8	4.6 ± 0.7	5.3
2.410 (514.5 nm) (Ref. [4])	4.3 ± 0.6	6.1 ± 0.8	4.4 ± 0.3	5.8

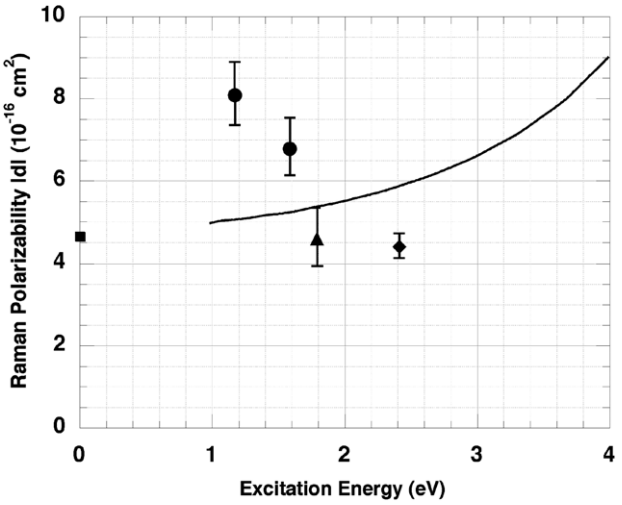

Fig. 6. Plot of the Raman polarizability $|d|$ *vs.* excitation energy. The excitation-energy-dependent computed values (solid curve), the computed static value (square), the measured values (circles), data of Ref. [3] (triangle), and the data of Ref. [4] (diamond) are shown.

well described by the density functional theory [3]. So we expect our theoretical Raman intensities to be reasonably accurate, given the level of uncertainty of the experimental results.

Fig. 6 shows a plot of the computed values of $|d|$ vs. excitation energy using TDDFT; the measured values of $|d|$ are also shown in Fig. 6. In general, TDDFT calculations in the LDA approximation can have problems to reproduce some properties of extended systems, in particular the band gap and excitonic effects [37]. For diamond, however, the predicted dielectric function is very close to the experimental one, especially for low frequencies [2]. So we expect our theoretical results to be reasonably accurate, given the level of uncertainty of the experimental results.

Our theoretical calculations confirm that the sign of d is positive, in agreement with that reported by Go et al. [38] and Cardona [39]. The positive sign of d implies that the polarizability increases with the increase of the bond length. This suggests that the effective induced charge increases with the increase of the bond length. Hence, diamond lies on the left-hand side of the peak in the so-called Laffer curve for the effective induced charge vs. bond length, similar to GaAs in the Laffer curve for the effective charge vs. lattice parameter [40].

To estimate the contribution of IaA and IaB defects to Raman polarizability, we have computed the Raman response of 64-atom diamond supercells with single IaA and IaB defects in the long-wavelength limit. Thus, the actual concentration of nitrogen atoms in the computed structures is several times higher than in the experiments. The change in the Raman polarizability associated with the defects is smaller than 5%. At this point we can conclude from theoretical calculations that the impurity effects cannot account for the difference between the experimentally measured data for type Ia and type IIa diamonds.

5. Conclusions

Our measured values of the absolute Raman scattering cross sections of type Ia diamond for 785- and 1064-nm excitation, obtained using a temperature-controlled blackbody for the signal calibration of the Raman spectrometers, are somewhat larger than the computed values obtained using time-dependent density functional theory in the local density approximation. Our measured and computed values of $|d|$ are somewhat larger ($<2\times$) than those in Refs. [3,4] for type IIa diamonds.

Acknowledgments

We thank Peter O'Brien for providing the diamond sample, Dan Calawa for X-ray orientation of the sample, Jon Wilson for the UV-V-NIR absorption spectrum, and Dr. T.Y. Fan for his comments on this paper. The MIT Lincoln Laboratory portion of this work was sponsored by the Defense Advanced Research Projects Agency under Air Force Contract FA8721-05-C-0002. The work at Harvard University was sponsored by the Defense Advanced Research Projects Agency under Air Force Contract FA9550-08-1-0285, by the Defense Threat Reduction Agency under Contract No. HDTRA1-10-1-0046, and by the National Science Foundation "Solar" Award DMR-0934490. Opinions, interpretation, and recommendations are those of the authors, and do not necessarily represent the view of the United States Government.

References

[1] R.L. Aggarwal, L.W. Farrar, D.L. Polla, Solid State Commun. 149 (2009) 1330.
[2] G.F. Bertsch, J.-I. Iwata, A. Rubio, K. Yabana, Phys. Rev. B 62 (2000) 7998.
[3] N. Mounet, N. Mazari, Phys. Rev. B 71 (2005) 205214.
[4] A.K. McQuillan, W.R.L. Clements, B.P. Stoicheff, Phys. Rev. A 1 (1970) 628.
[5] M.H. Grimsditch, A.K. Ramdas, Phys. Rev. B 11 (1975) 31030.
[6] In 1822 Friedrich Mohs chose 10 well known minerals and arranged them in order of their scratch hardness in decending order: diamond (10), sapphire (9), topaz (8), quartz (7), orthoclase feldspar (6), apatite (5), fluorspar (4), calcite (3), gypsum (2), and talc (1).
[7] The National Bureau of Standards (now NIST) developed the Knoop hardness in 1939.
[8] C.A. Klein, G.F. Cardinale, Proc. SPIE 1759 (1992) 178.
[9] S. Logothetidis, J. Petalas, H.M. Polatoglou, D. Fuchs, Phys. Rev. B 46 (1992) 4483.
[10] E.D. Palik (Ed.), Handbook of Optical Constants of Solids, Academic Press, 1985, p. 565.
[11] See, for example, Thermophysical Properties of Matter, The TPRC Data Series, vol. 2 (1971).
[12] See, for example C. Kittel, Introduction to Solid State Physics, eighth ed., John Wiley & Sons, New York, 2005, p. 16.
[13] S.A. Solin, A.K. Ramdas, Phys. Rev. B 1 (1970) 1687.
[14] E. Anastassakis, E. Burstein, Phys. Rev. B 6 (1970) 1952.
[15] Edmund Optics, Barrington, NJ 08007-1380, USA.
[16] Chroma Technology Corp., Rockingham, VT 05101, USA.
[17] Sacher Lasertechnik, Marburg, Germany, Buena Park, CA 90620, USA.
[18] IPG Photonics, Oxford, MA 01540, USA.
[19] DeltaNu, Laramie, WY 82020, USA.
[20] Intevac, Inc., Santa Clara, CA 95054, USA.
[21] Electro Optical Industries, Santa Barbara, CA 93111, USA.
[22] R. Loudon, Adv. Phys. 13 (1964) 423.
[23] See, for example S. Bhagavantam, Crystal Symmetry and Physical Properties, Academic Press, London, New York, 1966, p. 11.
[24] P. Giannozzi, et al., J. Phys.: Condens. Matter 21 (2009) 395502.
[25] M. Lazzeri, F. Mauri, Phys. Rev. Lett. 90 (2003) 036401.
[26] A. Castro, M. Marques, H. Appel, M. Oliveira, C. Rozzi, X. Andrade, F. Lorenzen, E. Gross, A. Rubio, Phys. Status Solidi B 243 (2006) 2465.
[27] For both codes, we used the C.pz-vbc.UPF and N.pz-vbc.UPF. Pseudopotentials from: http://www.quantum-espresso.org.
[28] H. Wendel, Solid State Commun. 31 (1979) 423.
[29] S. Baroni, R. Resta, Phys. Rev. B 33 (1986) 5969.
[30] G.B.B.M. Sutherland, D.E. Blackwell, W.G. Simeral, Nature 4437 (1954) 901.
[31] C.D. Clark, E.W.J. Mirchell, B.J. Parsons, in: J.E. Field (Ed.), Properties of Diamond, Academic Press, London, 1979, pp. 23–77.

[32] G.S. Woods, G.C. Purser, A.S.S. Mtimkulu, A.T. Collins, J. Phys. Chem. Solids 51 (1990) 1191.
[33] T. Evans, C. Phaal, Proc. R. Soc. Lond. Ser. A 270 (1962) 538.
[34] R.L. Aggarwal, L.W. Farrar, S.K. Saikin, A. Aspuru-Guzik, M. Stopa, D.L. Polla, Solid State Commun. 151 (2011) 553.
[35] X. Andrade, S. Botti, M.A.L. Marques, A. Rubio, J. Chem. Phys. 126 (2007) 184106-8.
[36] K.F. Young, H.P.R. Frederikse, J. Phys. Chem. Ref. Data 2 (1973) 313.
[37] G. Onida, L. Reining, A. Rubio, Rev. Modern Phys. 74 (2002) 601.
[38] S. Go, H. Bilz, M. Cardona, Phys. Rev. Lett. 34 (1975) 580.
[39] M. Cardona, Light Scattering in Solids II, in: Topics Appl. Phys., vol. 50, Springer-Verlag, Berlin, Heidelberg, New York, 1982, p. 19.
[40] M. Cardona, 2002, p. 19. arXiv:cond-mat/0204606v1 [cond-mat-mtrl-sci].